Numerical study of sediment dynamics during Hurricane Gustav

Zhengchen Zang[a], Z. George Xue[a,b,c *], Shaowu Bao[d], Qin Chen[b,c,e], Nan D. Walker[a,c], Alaric S. Haag[a,c], Qian Ge[f], and Zhigang Yao[g]

a. Department of Oceanography and Coastal Sciences, Louisiana State University, Baton Rouge, LA 70803, USA
b. Center for Computation and Technology, Louisiana State University, Baton Rouge, LA 70803, USA
c. Coastal Studies Institute, Louisiana State University, Baton Rouge, LA 70803, USA
d. School of Coastal and Marine Systems, Coastal Carolina University, Conway, SC 29528, USA
e. Department of Civil and Environmental Engineering, Louisiana State University, Baton Rouge, LA 70803, USA
f. Second Institute of Oceanography, SOA, Hangzhou, China
g. Key Laboratory of Physical Oceanography, Ocean University of China, Qingdao, China

Corresponding to:
Z. George Xue
Dept. of Oceanography and Coastal Sciences, Louisiana State University, Baton Rouge, LA 70803
Tel: (225) 578-1118, Fax: (225) 578-6513, Email: zxue@lsu.edu

Abstract

In this study, the Coupled Ocean-Atmosphere-Wave-and-Sediment Transport (COAWST) modeling system was employed to explore sediment dynamics in the northern Gulf of Mexico during Hurricane Gustav in 2008. The performance of the model was evaluated quantitatively and qualitatively against in-situ and remote sensing measurements, respectively. After Gustav's landfall in coastal Louisiana, the maximum significant wave heights reached more than 8 m offshore and they decreased quickly as it moved toward the inner shelf, where the vertical stratification was largely destroyed. Alongshore currents were dominant westward on the eastern sector of the hurricane track, and offshoreward currents prevailed on the western sector. High suspended sediment concentrations (> 1000 mg/l) were confined to the inner shelf at surface layers and the simulated high concentrations at the bottom layer extended to the 200-m isobaths. The stratification was restored one week after landfall, although not fully. The asymmetric hurricane winds induced stronger hydrodynamics in the eastern sector, which led to severe erosion. The calculated suspended sediment flux (SSF) was convergent to the hurricane center and the maximum SSF was simulated near the south and southeast of the Mississippi River delta. The averaged post-hurricane deposition over the Louisiana Shelf was 4.0 cm, which was 3.2–26 times higher than the annual accumulation rate under normal weather conditions.

Keywords: COAWST, Cohesive sediment, Gulf of Mexico, Sediment Flux

1. Introduction

The Mississippi River is the seventh largest river globally in terms of its sediment flux (Meade and Moody, 2010; Allison et al., 2012), where it delivers ~115 Mt of sediments per year to the northern Gulf of Mexico (nGoM). The combined high fluvial sediment discharge, relatively steady sea level, and modest wave and tide energy have resulted in the relatively rapid progradation of the bird-foot delta over the past 7500 years (Coleman et al., 1998; Xu et al., 2011). The deposition of sediments in the Mississippi delta has been highly localized, and the accumulation rate is in the order of the cm/yr level (Allison et al., 2007; Osterman et al., 2009). The fluvial sediments settled quickly around the delta plain and only a small portion could reach the shelf break in normal conditions (Dail et al., 2007), whereas under severe weather conditions, such as tropical cyclones (hurricanes), the deposited sediments could be resuspended by intensified bottom shear stress and the thickness of the post-hurricane deposition could be up to 19 cm (Goñi et al., 2006). The nGoM region is hit by hurricanes and tropical storms every 3 years on average (Keim et al., 2007). Records of event-driven erosion and deposition have been captured based on sediment cores from coastal woodland to shelf break, which exhibited upward fining sequences (Turner et al., 2006; Goñi et al., 2006, 2007; Dail et al., 2007; Williams and Flanagan, 2009; Liu et al., 2011). Radionuclide analysis (e.g., ^{7}Be, ^{137}Cs, ^{234}Th, and ^{210}Pb) also indicates that the post-hurricane deposition mainly comprised resuspended material from previously deposited sediments, and that storm mudflows are capable of exporting sediments out of the delta front (Corbett et al., 2004; Allison et al., 2005; Goñi et al., 2006; Walsh et al., 2006). In addition, understanding shelf sediment transport processes during hurricanes is important in terms of coastal engineering and marine ecosystem. For example, in 1969, the strong storm waves associated with Hurricane Camille triggered landslides and damaged three oil platforms around the Mississippi Delta (McAdoo et al., 2000). More recently, the mudslides induced by Hurricane Ivan (2004) and Katrina (2005) caused severe damage to pipelines in the nGoM (Nodine et al., 2007). In addition, from an ecosystem perspective, the high precipitation caused by hurricanes can increase the export of dissolved organic matter and influence the biogeochemical processes and water quality in nearshore areas (Yoon and Raymond, 2012).

Hurricanes can induce dramatic changes in the water level (Chen et al., 2008; Sheng et al., 2010), surface temperature (Shay et al., 1992; Walker et al., 2005), vertical structure of the water column (Zambon et al., 2014), and other variables (Hu and Chen, 2011). In addition, changes in the ocean conditions can affect hurricanes, and modulate their intensity and movement (Bender and Ginis, 2000; Waker et al., 2005; Liu et al., 2011). Understanding the hydrodynamics during hurricane events as well as their impacts on sediment dynamics is still very challenging due to the difficulties related to obtaining in-situ measurement (Lapetina and Sheng, 2015). Remote sensing can capture the extension and development of elevated surface suspended sediments (Walker and Hammack, 2000; Palaseanu-Lovejoy et al., 2013), but the availability and quality of these data are largely compromised by thick clouds and water vapor.

Numerical model is an alternative option for investigating ocean conditions and their impacts on sediment dynamics during hurricane events. Olabarrieta et al. (2012) adapted the Coupled Ocean-Atmosphere-Wave-and-Sediment Transport (COAWST; Warner et al., 2010) modeling system for Hurricane Ida and Nor'Ida in the Gulf of Mexico during 2009, where they demonstrated that the asymmetry of the low-pressure vortex were influenced mainly by wave-induced sea surface roughness. The wind speeds and wave heights became smaller due to feedback between the atmosphere and wind-waves. Using parametric wind fields, Liu et al. (2015) adapted a sediment transport model to Delft3D (Lesser et al., 2004) and simulated an average ~4 cm-thick post-hurricane deposition in coastal wetlands after the landfall of Hurricane Gustav in 2008. Under driving by wind fields from a parametric hurricane wind model, Xu et al. (2016) adapted the Regional Ocean Modeling System (ROMS; Shchepetkin and McWilliams, 2005; Haidvogel et al., 2008) to the nGoM for Hurricanes Katrina and Rita in 2005, and found that the spatial patterns of erosion and deposition were influenced by the hurricane tracks, bed shear stress, grain sizes, and bathymetry.

In this study, we employed numerical modeling to investigate the ocean conditions and sediment dynamics in the nGoM during Hurricane Gustav, which was the seventh tropical storm and the third hurricane in 2008. Gustav first appeared as a tropical wave in the Lesser Antilles and grew quickly from a tropical depression to a hurricane in less than 12 h (Beven and Kimberlain, 2009). Gustav reached its peak intensity upon landing in western Cuba. Subsequently, it gradually became weaker after entering the Gulf of Mexico because of increased wind shear and dry air intrusion (Forbes et al., 2010). On September 1, 2008, Gustav made landfall near Cocodrie, Louisiana as a Category 2 hurricane. It then decayed into a tropical storm during its slow movement across Louisiana (Forbes et al., 2010). Using a three-way (ocean-wave-atmosphere) coupled sediment transport model, the objectives of this study were: 1) to understand the spatial and temporal extent of the disruption of the hydrodynamics and deltaic deposits on a continental shelf (e.g., the nGoM) due to land-falling hurricane by using Gustav as an example; 2) to semi-quantitatively evaluate the impact of a land-falling hurricane on alongshore and cross-shore sediment transport; and 3) to examine the impacts of hydrodynamic asymmetry along the two sides of a hurricane on the sediment dynamics.

2. Model Setup

We adapted the open source COAWST model (Warner et al., 2008 and 2010, https://woodshole.er.usgs.gov/operations/modeling/COAWST) to the Gulf of Mexico waters (Fig. 1). COAWST is an open source community model that incorporates three state-of-the-art numerical models (the Weather Research and Forecasting model [WRF, v 3.7.1, Skamarock et al., 2005], ROMS [svn 797, Haidvogel et al., 2008; Shchepetkin and McWilliams, 2005], and the Simulating Waves Nearshore model [SWAN, v 41.01AB, Booij et al., 1999]). COAWST uses the Model Coupling Toolkit (MCT; Jacob et al., 2005) and the Spherical Coordinate Remapping Interpolation Package (SCRIP; Jones, 1997) to support variable exchanges between different models. In addition, COAWST provides a comprehensive MATLAB® toolbox to prepare the necessary model inputs (e.g., ocean initial and boundary conditions). For the sediment module, the Community Sediment Transport Modeling System (CSTMS; Warner et al., 2008) was integrated into the ocean model. The sediment routines employed multiple algorithms to simulate suspended sediment transport and bed load transport, and the incorporated seabed modules could track the stratigraphy, morphology, and seabed consolidation (Warner et al., 2010). In this study, we conducted an 11-day three-way (ROMS-SWAN-WRF) coupled sediment transport simulation of Hurricane Gustav (August 30–September 9, 2008). Details of the model setup are described in the following.

2.1. Ocean-Sediment Transport model (ROMS-CSTMS)

The ocean model domain covered the entire Gulf of Mexico at a 5-km horizontal resolution. We focused on the nGoM region where the riverine and deltaic deposition is most abundant (Fig. 1). Vertically, there were 36 terrain-following sigma layers. For an open boundary, the Orlanski-type radiation condition was imposed, combined with temperature and salinity nudging toward the Hybrid Coordinate Ocean Model solutions (HyCOM/NCODA GLBu0.08, https://hycom.org; 1/12° resolution; Chassignet et al., 2003). A gradient boundary condition was applied to sediment tracers and the sea-free surface. Depth-averaged current velocity boundary conditions were specified according to Flather (1976). Tidal forcing was derived from the Oregon State University (OSU) Tidal Inversion Software (OTIS) regional tidal solution (Egbert and Erofeeva, 2002). Initial conditions (sea-level, hydrodynamics, temperature, and salinity) were extracted from the HyCOM reanalysis for August 30, 2008. Water discharge and sediment concentration data for 39 rivers were retrieved from USGS gages (http://nwis.waterdata.usgs.gov) and specified at the land-ocean boundary. The temperature field was nudged to the HyCOM-derived climatology every three days to provide a better bottom boundary condition for the atmospheric model.

For the sediment model (CSTMS), we defined two cohesive and one non-cohesive sediment class for river input, and the percentage of each component was based on measurements by Mickey et al. (2015). Sediment fractions on the seabed were extracted from historical surficial grain-size data provided by the usSEABED project (Buczkowski, 2006; Fig. 2). To achieve an equilibrium initial condition for sediment fields, we first performed a two-way coupled (SWAN-ROMS with CSTMS) simulation starting from January 1, 1993 and then extracted the model output on August 30, 2008 as the initial sediment condition (more details of the model setup are given in Supplementary Files). The sediment model was parameterized according to two previous nGoM sediment modeling studies by Xu et al. (2011 and 2016; Table 1).

Considering the high percentage of cohesive particles in the study region and intensive seafloor scour during hurricanes (Balsam and Beeson, 2003; Ellwood et al., 2006; Dail et al., 2007; Teague et al., 2007; Turner et al., 2007), we set 40 sediment layers with a total thickness of 1 m (2.5 cm for each) to resolve the sediment bed variability. We applied the cohesive algorithm so the critical shear stress of the sediment layers increased downward by following an asymptotic line to represent the effect of self-weight consolidation (Parchure and Mehta, 1985; Rinehimer et al., 2008). The equilibrium critical shear stress profile was designed as follows:

$$\tau_{cr(k)} = exp\left(\frac{(log(M_{k-1}) - tcr\_off)}{tcr\_slp}\right), \qquad (1)$$

where $\tau_{cr(k)}$ is the bed critical shear stress in layer k, M_{k-1} is the total bed mass from the top sediment layer to layer k–1, and tcr_off and tcr_slp are unitless constants. We constructed the $\tau_{cr\,(k)}$ profile according to Rinehimer et al. (2008) in order to represent sediment resuspension (see Fig. 3).

2.2. Wave model (SWAN)

The SWAN model was employed to simulate the wind-wave generation and propagation processes. SWAN is based on a Eulerian formulation of the discrete spectral balance of action density that accounts for refractive propagation over arbitrary wind and current fields (Booij et al., 1999; Chen et al., 2005). In our simulations, the SWAN model shared the same grid as the ROMS model and its surface wind was fed by the atmospheric model. The ratio of the maximum individual wave height relative to the depth was 0.73, and the proportionality coefficient of the rate of dissipation was 1.0. Bottom friction was calculated using the formulations given by Madsen et al. (1988).

2.3. Atmospheric model (WRF)

WRF (ARW core, version 3.7.1) was employed to represent atmospheric conditions (Skamarock et al., 2005). The WRF grid dimension was 429 by 429 with 6-km horizontal resolution (Fig. 1). The single-moment six-class microphysics scheme was implemented, which features water vapor, cloud water, cloud ice, rain, snow, and graupel (Hong and Lim, 2006). The Rapid Radiative Transfer Model for general circulation models (RRTMG) Shortwave and Longwave Schemes (Iacono et al., 2008) was employed to compute the longwave and shortwave radiation physics, where it was called every 6 min on the grid. The Eta Similarity Scheme (Janjic, 2002) and Unified Noah land surface model (Tewari et al., 2004) were selected. The WRF model was initialized using the 1° Global Forecasting System (http://www.emc.ncep.noaa.gov/GFS) developed by the National Centers for Environmental Prediction (http://www.ncep.noaa.gov). To obtain satisfactory initial conditions, we ran WRF alone starting at 00:00:00 UTC, August 29. After spin up for 24 h, the tropical cyclone was well formed and balanced with other fields. After initialization, the ERA Interim atmospheric model result (ERA-Interim, https://www.ecmwf.int/en/research/climate-reanalysis/era-interim) was applied as the boundary condition. No nudging or data assimilation was used in the three-way coupled simulation.

2.4. Model coupling

Model coupling and interpolation were performed using MCT and SCRIP as part of the COAWST model. In our setup, ROMS sent the sea surface temperature to WRF, and the sea surface height (SSH) and vertically averaged currents to SWAN. Our simulation employed a wave-current bottom boundary layer model (SSW_BBL; Madsen, 1994), which considered the effect of wave-enhanced bottom stress on the momentum bottom boundary condition for the Reynolds-averaged Navier–Stokes equations. The bottom roughness comprised the sum of the grain roughness, sediment transport roughness, and bedform roughness. WRF and SWAN then sent the atmospheric forcing (heat flux and sea surface stress) and sea surface wave parameters (e.g., significant wave height, wavelength, relative peak period, and dissipation energy) to ROMS. Surface winds from WRF were used by SWAN to calculate the significant wave height and wave period, which were then used to estimate the sea surface roughness in WRF (Taylor and Yelland, 2001). The sediment concentration was not included in the water density equation. Morphological changes due to sediment were not considered in order to avoid instability in our model. Exchanges of the variables among the three models occurred at an interval of 600 s.

We designed several experiments to verify the sensitivity of the model to wave–current interactions during the hurricane simulation, including the three-dimensional vortex force and the Bernoulli Head, wave breaking-induced accelerations and turbulence injection, and wave-enhanced vertical viscosity mixing (Uchiyama et al., 2010; Olabarrieta et al., 2011; Kumar et al., 2012). The wind speed, significant wave height, and water level were evaluated quantitatively in each test based on the Willmott model skill (Willmott, 1982), and the results did not indicate any substantial differences (model skill difference < 0.01) when wave–current interactions were included. In addition, we conducted a domain-wide comparison of the current speed, significant wave heights, and suspended sediment concentrations (SSC), and only found very trivial differences. The limited effect of wave–current interactions may be attributed to the relatively coarse spatial resolution of the coastal area, where wave-driven littoral currents and undertows were most salient. This study focused mainly on the sediment dynamics on the nGoM shelf, so our analysis was based on the results from the benchmark run where the aforementioned wave–current interaction processes were not incorporated.

3. Results and Discussion

3.1. Model calibration

We compared the outputs of the three models against observations to evaluate the performance of our hurricane simulation. As shown in Fig. 4, the model-simulated hurricane track agreed well with the observed track. The model-simulated track diverted slightly to the west after September 1 and it resulted in a westward shift of the landfall location by 30 km. The model's simulations of the wind speed, air pressure, significant wave height, and sea level captured the observed variations at the National Data Buoy Center buoy stations and the National Oceanic and Atmospheric Administration (NOAA) tidal gauges (see Fig. 1 for the locations of the tidal gauges and buoy stations) during the hurricane. The data correlation coefficients for the model-observation comparison ranged from 0.81 to 0.98. As Gustav approached, the wind speed (Figs. 5a, 5b, and 5c) and significant wave height (Figs. 5d, 5e, and 5f) increased sharply whereas the air pressure dropped substantially (Figs. 5g, 5h, and 5i). Changes in the sea level were largely localized depending on the quadrant relative to the hurricane. At stations 8735180 and 8727520 to the east of the hurricane track, the sea level increased by ~ 0.5–1.1 m during the passage of the hurricane (Fig. 5k and 5l), and a higher frequency signal was found at Station 8772447 to the west of the hurricane (Fig. 5j). The good agreement between the model and observations allowed us to be confident that the coupled model was capable of reproducing hurricane-induced changes in the ocean conditions.

No in-situ SSC measurements were available during Gustav, so we qualitatively compared the surface SSC simulated by the model with a partially cloud-free MODIS Terra image obtained at 16:30:00 UTC on September 2, 2008 (Fig. 6). No quantitative comparison was conducted because attempts to derive SSC from the MODIS images failed due to their poor quality. We analyzed a large amount of satellite raw data and the image in Fig. 6 had the best quality. The model and satellite image indicated high turbidity in the waters west of the "bird-foot" delta. The SSC decreased sharply toward the outer shelf in the south. Compared with the MODIS image, the extension of the SSC simulated using the model was more widespread. We attributed this discrepancy to: 1) the availability of satellite data (only one snap-shot was available, which may or may not have represented the in-situ conditions for a relatively long period, e.g., up to hours); 2) the sensitivity of the model to different parameters, especially the settling velocity, which requires further study. Nevertheless, our model was capable of capturing the southeastward sediment plume along the southern limit of the high turbid water. In addition, the storm layer thickness simulated by the model was comparable to that reported in previous studies, where it was usually less than 20 cm (Keen et al., 2004; Allison et al., 2005; Goñi et al., 2006, 2007; Palinkas et al., 2013; Xu et al., 2016).

3.2. Ocean conditions and suspended sediment distributions

The simulated wind speed reached more than 40 m/s when Gustav made landfall. The wind direction varied substantially in different quadrants relative to the vortex (northerly wind to the west and southerly wind to the east; Fig. 7a). The wind speed decreased sharply after moving away from the center of the vortex. The maximum wave height occurred to the east of the hurricane track, where it reached more than 8 m (Fig. 7a). In coastal areas (water depths < 20 m), the wave heights dropped sharply to less than 2.5 m even in the presence of strong winds (> 35 m/s; Fig. 7a). This pattern was very similar to that reported by Stone et al. (1995) and Xu et al. (2016), which could be explained by the peak wave energy dissipation around the 25–30 m contours on the Mississippi River subaqueous delta. Previous studies reported a positive correlation between wave dissipation and sediment resuspension during hurricane events, which would be further strengthened in the Mississippi delta due to the soft and muddy seafloor (Sheremet et al., 2005; Elgar and Raubenheimer, 2008).

The currents exhibited great spatial variability in different quadrants relative to the hurricane track during strong winds (Fig. 7b). Alongshelf currents were prevalent to the east of the track and they flowed toward the west. The speed of these alongshelf currents could be up to 2.1 m/s (Fig. 7b). By contrast, to the west, the currents turned to a south- and southeastward (offshoreward) direction with a speed of ~1.2 m/s. Strong bottom shear stress (> 6 Pa) was found near the bird-foot delta where the water depth was shallower than 50 m (Fig. 7b).

During Gustav, the simulated SSC reached 10,000 mg/l in both the surface and bottom layers on the shelf. The spatial limits of high turbidity water largely followed the 50-m isobaths at the surface layer and 200-m isobaths for the bottom layer (Figs. 7c and 7d). The distribution of the high surface SSC matched that of the strong bottom shear stress, while high bottom SSC was prevalent, especially over the shelf between 89°W and 93°W.

We calculated the temporal variation in the spatial (nGoM) averaged bottom shear stress induced by currents and waves, and the total bed thickness. The wave and current induced bottom shear stresses increased dramatically after September 1 and reached their peak values (0.64 N/m^2 and 0.20 N/m^2, respectively) when Gustav made landfall. Subsequently, the bottom shear stress recovered to normal conditions within 2 days. The maximum spatial averaged erosion depth in the nGoM was 2 cm, and ~50% of the resuspended sediments settled back to the seabed by around 10:00:00 UTC on September 3 (Fig. 8). After 60 h more, the percentage reached 80%. On September 9, ~ 90% of the resuspended sediments had returned to the seabed. Soon after, another major hurricane called Ike entered the nGoM and made landfall in Texas on September 13, 2008.

3.3. Variations in vertical structure

During Gustav, the wind speed and wave height began to increase from 00:00:00 UTC on August 31, before reaching their peak values around 16:00:00 UTC on September 1, and then returning to normal conditions around 00:00:00 UTC on September 9 (Fig. 5). We extracted the temperature, salinity, and SSC fields along the 50-m isobath transect (the position is shown in Fig. 1b) at these three times to plot their vertical structures in the pre-, during, and post-hurricane stages, respectively (Fig. 9). We used the Brunt Väisälä Frequency (BVF) to estimate the intensity and depth of the pycnocline (Fig. 9). The mean BVF at a given depth (N) is given by:

$$N = \sqrt{-\frac{g}{\rho} \cdot \frac{d\rho}{dz}} \;, \qquad (2)$$

where g = 9.81 m/s^2 is the acceleration due to gravity, ρ is the spatial mean potential density of the water along the 50-m isobath transect at a certain depth, and $\frac{d\rho}{dz}$ is the vertical potential density gradient. We excluded water density variations due to SSC and the estimated BVF only represented the vertical stratification induced by the water itself, and not by the water/sediment mixture.

As shown in Fig. 9a, before the landfall of Gustav, the water was well stratified and the temperature dropped gradually with the depth from 32°C to 20°C. The water temperature was low (<25°C) near the Southwest Pass of the Mississippi delta, which connects to the shelf water through a submarine canyon. The salinity increased with depth, where it ranged from 26 to 38 PSU (Fig. 9d). Low salinity water was found mostly around the Mississippi River mouth due to the large input of freshwater. High SSC (~ 100 mg/l) was simulated at the bottom close to the Mississippi River mouth (Fig. 9g). BVF calculations identified a strong pycnocline in the sub-surface layer (7 m below surface; Fig. 10). Another salient density stratification with higher intensity was detected near the bottom. The transect-averaged SSC was maximized at the bottom with a magnitude of 100 mg/l.

After the landing of Gustav, the transect-averaged temperature decreased by ~2°C (9b). Stratification was largely destroyed due to strong vertical mixing (Fig. 9e). The only exception was at the west end 150 km away from the landing site. Freshwater from the Atchafalaya Bay flushed offshore and generated a low-salinity transect, which was 150 km wide and 40 m deep (Fig. 9e; Walker, 2001). SSC increased dramatically with the hurricane's passage and reached more than 1,000 mg/l in the water column (Figs. 9h, and 10). Compared with the pre-hurricane stage, the sub-surface pycnocline was thoroughly destroyed, whereas the strength of the near bottom density stratification remained largely unchanged (Fig. 10). The SSC profile exhibited limited vertical variation with a mean value of 830 mg/l throughout the water column.

One week after Gustav landed (00:00:00 UTC, September 9), the sea surface temperature had not recovered from the hurricane-induced cooling (Fig. 9c). The low salinity river plume near the Mississippi River's Southwest Pass could be identified again (Fig. 9f). The surface SSC decreased dramatically after Gustav landed, but a higher SSC remained at the bottom than that in the pre-hurricane stage (Fig. 9i). A weak sub-surface pycnocline was found, and the transect-averaged SSC decreased throughout the water column, although it was still higher than that in the pre-hurricane stage (Fig. 10). The sediment and temperature were still different from those in the pre-hurricane stage, but more than 90% of the resuspended sediments had already settled on the seabed, before another hurricane called Ike (2008) entered the Gulf of Mexico and induced another round of resuspension. Therefore, the post-hurricane condition in this study did not represent 100% restoration.

3.4. Asymmetric transport during the hurricane

Highly intensified short-term events (e.g., hurricanes, floods, and winter storms) are capable of substantially disrupting shelf deposition (Liu and Fearn, 1993; Turner et al., 2006). A unique feature of hurricane-induced sediment transport is the asymmetry on different sides of the vortex. During hurricanes, the highest wind speed is found to the right of the track (Price, 1981; Xie et al., 2011; Uhlhorn et al., 2014), which leads to an asymmetric pattern in the hydrodynamics, including strong currents and waves in a shoreward direction to the right but relatively weak winds, currents, and waves to the left. The current fields in Fig. 7b illustrate the offshore (southward-southeastward) currents from Atchafalaya Bay after joining together with the strong alongshore currents from the eastern coastal Louisiana, where they moved southeastward continuously into the open gulf. The highly intensified alongshore and offshore currents were capable of transporting large amounts of sediment far from where they originally deposited. Wave–current interactions were not considered in this study, but previous studies have highlighted the importance of wave-induced littoral currents and undertows, as well as their effects on sediment transport. Uchiyama et al. (2010) stated that the littoral currents caused by wave breaking are maximized near the topographic bar, and that the sediment transport induced by wave–current interactions in coastal regions is important for sandbar migration (Hoefel and Elgar, 2003; Hsu et al., 2006). Olabarrieta et al. (2011) found that the wave-generated current patterns varied greatly in the inlet zone. In addition, wave–current interactions have critical effects on the horizontal and vertical structure of fresh water plumes, which is important for coastal sedimentation (Rong et al., 2014).

In order to examine this asymmetric pattern as well as its impact on sediment transport, we grouped and averaged the modeling results according to their sides relative to the track after Gustav's landfall (16:00:00 UTC, September 1; Fig. 11). Waves play a vital role in sediment resuspension during the shoaling of a hurricane (Thornton and Guza, 1983; Miles et al., 2015). The maximum significant wave heights (~ 7 m) simulated by the model occurred in the eastern sector (Figs. 7a and 11b) due to the strong winds and shoreward wave piling up (Figs. 7a and 11a). At the vortex center, the wave height dropped to less than 2 m, with a greatly reduced wind speed (< 15 m/s; Figs. 11a and 11b). By contrast, the surface currents were greatly intensified in the center of the vortex and they were generally stronger on the east side (0.6–1.3 m/s) than the west side (0.2–1.3 m/s; Fig. 11c). Several studies have emphasized that the sediment transport during hurricanes is mainly due to resuspension caused by increased bottom shear stress (Ogston and Sternberg, 1999; Keen and Glenn, 2002; Miles et al., 2015). According to our simulation, the bottom shear stress induced by waves was higher than that by currents, where it reached 3.6 Pa to the east. Both the wave and current induced shear stresses increased near the center of the vortex due to the strong hydrodynamics and relatively small water depth (Figs. 11d, 11e, and 11f). The high shear stress to the east led to high SSC and severe erosion (Figs. 7b, 7c, 7d, 11g, and 11h).

The maximum erosion was 0.13 m in the eastern sector, and the SSC in both the surface and bottom layers peaked at the same location (15.2 and 12.0 g/l, respectively). The spatial distribution pattern confirmed that the previously deposited sediments were the main source of the high SSC during the hurricane.

3.5. Suspended sediment flux (SSF)

To assess the SSF during Gustav, we calculated the depth-integrated and time-averaged (August 30–September 9, 2008) SSF using the velocity and SSC as follows:

$$SSF = \sum_{i=1}^{N} SSC_i \cdot u_i \cdot h_i \ , \qquad (3)$$

where *SSF* is the suspended sediment flux (unit: kg/m/s), SSC_i and u_i are the SSC (unit: g/l) and current speed (unit: m/s) in the i^{th} layers, respectively, *N* is the number of vertical layers (36 in this study), and *h* represents the thickness of each layer (unit: m).

The SSF was along the coastline and convergent along the inner shelf to the west of the hurricane track. The SSF was higher to the right of the track than the left, mainly due to the high SSC around the delta (Fig. 12). The maximum SSF was located to the south and southeast of the Mississippi River delta, where it reached ~11 kg/m/s. Erosion, deposition, and sediment transport mainly occurred over the inner shelf (< 50 m, Fig. 12). As the water depth increased to 200 m, the net erosion/deposition became trivial (<1 cm), thereby indicating that offshore sediment transport out of the shelf was limited. In contrast to the results obtained by Xu et al. (2016) for Katrina and Rita in 2005, Gustav induced less offshore transport to deep water (> 200 m). Strong offshore SSF was simulated over the wide and gentle continental shelf south and southwest off the Mississippi River delta. The SSF kept decreasing until the shelf break was reached. A depo-center with a thickness of 14 cm was simulated to the southwest of the hurricane track. Two sources were identified for this hurricane-driven deposition comprising sediments eroded from: (1) the south of the Mississippi River delta, and (2) the broad Louisiana-Texas shelf in the northwest. According to our SSF estimation, the first source (deltaic) provided more sediment because (1) sufficient material was deposited near the delta lobe, and (2) energetic ocean conditions to the right of the hurricane track. Another depo-center was found southeast of the Mississippi River delta between the 50-m and 200-m isobaths. This elongated deposition was formed by the offshore transport of sediments from the inner shelf. However, we advise caution as both the SSF and post-hurricane deposition estimations were relatively conservative because ~10% of the Gustav-induced resuspension was still present in the water column (Fig. 8). The approach of Hurricane Ike made it very difficult to estimate the total SSF induced by Gustav.

Previous studies have demonstrated that the majority of the fluvial sediments will settle over the inner shelf and offshore transport is limited under normal conditions (e.g., Xu et al., 2011). During hurricane events, such as Karina and Rita in 2005, the hurricane-driven accumulation can be five times larger than the annual sediment supply from the Mississippi and Atchafalaya Rivers, and even 10 times greater compared with the annual, long-term accumulation during non-storm periods (Goñi et al., 2007). Based on our simulation, the mean post-hurricane deposition in coastal Louisiana (water depth < 100 m) was 4.0 cm, which was 3.2 to 26 times of the ^{210}Pb-derived annual accumulated thickness (0.15 to 1.24 cm; Osterman et al., 2009).

4. Conclusions

In this study, we adapted the COAWST modeling system to the Gulf of Mexico to study the variations in the ocean conditions and sediment dynamics during Hurricane Gustav in 2008. The favorable model–data comparisons obtained, including the sea level, significant wave height, wind speed, air pressure, and surface sediment distribution, confirmed the feasibility of using a coupled model to investigate physical and sedimentary conditions during a hurricane event.

Water stratification on the inner shelf was completely destroyed by vertical mixing after Gustav's landfall. Large amounts of sediments were remobilized and brought to the surface layer (~ 1,000 mg/l). Eight days after landfall, sub-surface stratification appeared again but its intensity was less than that before Gustav landed. The hydrodynamics exhibited great spatial variability due to the asymmetric wind field. Stronger bottom shear stress and currents in the eastern sector resulted in massive sediment resuspension and transport. Severe seabed erosion, strong bottom shear stress, and high SSC were found where the peak wave energy dissipation rate occurred.

The calculated SSF reached 11 kg/m/s during the hurricane's passage and the direction of the SSF was convergent to the vortex center. The post-hurricane deposition rate was 3.2 to 26 times of that during normal ocean conditions. Two depo-centers were simulated with a maximum thickness of 14 cm after the passage of hurricane Gustav.

Acknowledgments

Research support provided through National Science Foundation (award number CCF-1539567; OCE-1635837), NOAA (award number NA16NOS4780204), Fund of China National Programme on Global Change and Air-Sea Interaction (Grant Nos. GASI-GEOGE-03 and GASI-04-01-02), and the National Natural Science Foundation of China (Grant Nos. 41476047 and 41106045) is much appreciated. We are grateful to Alfredo L. Aretxabaleta and John C. Warner of the US Geological Survey, Woods Hole, and Lilong Zhou of China Meteorological

Administration for their help with the model setup and suggestions regarding sediment and atmospheric simulations. Computational support was provided by the High Performance Computing Facility (cluster Supermike II) at Louisiana State University.

References

Allison, M.A., Bianchi, T.S., McKee, B.A., Sampere, T.P., 2007. Carbon burial on river-dominated continental shelves: Impact of historical changes in sediment loading adjacent to the Mississippi River. Geophys. Res. Lett. 34, 1–6. doi:10.1029/2006GL028362

Allison, M.A., Demas, C.R., Ebersole, B.A., Kleiss, B.A., Little, C.D., Meselhe, E.A., Powell, N.J., Pratt, T.C., Vosburg, B.M., 2012. A water and sediment budget for the lower Mississippi-Atchafalaya River in flood years 2008-2010: Implications for sediment discharge to the oceans and coastal restoration in Louisiana. J. Hydrol. 432–433, 84–97. doi:10.1016/j.jhydrol.2012.02.020

Allison, M.A., Sheremet, A., Goni, M.A., Stone, G.W., 2005. Storm layer deposition on the Mississippi-Atchafalaya subaqueous delta generated by Hurricane Lili in 2002. Cont. Shelf Res. 25, 2213–2232. doi:10.1016/j.csr.2005.08.023

Balsam, W.L., Beeson, J.P., 2003. Sea-floor sediment distribution in the Gulf of Mexico. Deep. Res. Part I Oceanogr. Res. Pap. 50, 1421–1444. doi:10.1016/j.dsr.2003.06.001

Bender, M.A., Ginis, I., 2000. Real-Case Simulations of hurricane – ocean interaction using a high-resolution coupled model : effects on hurricane intensity. Mon. Weather Rev. 128, 917–946. doi:10.1175/1520-0493(2000)128<0917:RCSOHO>2.0.CO;2

Beven, J.L., Kimberlain, T.B., 2009. Tropical Cyclone Report Hurricane Gustav (AL072008) 25 August–4 September 2008. Natl. Hurric. Cent. 22.

Booij, N., Ris, R.C., Holthuijsen, L.H., 1999. A third-generation wave model for coastal regions: 1. Model description and validation. J. Geophys. Res. Ocean. 104, 7649–7666.

Buczkowski, B.J., 2006. usSEABED: Gulf of Mexico and Caribbean (Puerto Rico and US Virgin Islands) offshore surficial-sediment data release. US Department of the Interior, US Geological Survey.

Chassignet, E.P., Smith, L.T., Halliwell, G.R., Bleck, R., 2003. North Atlantic simulations with the Hybrid Coordinate Ocean Model (HYCOM): Impact of the vertical coordinate choice, reference pressure, and thermobaricity. J. Phys. Oceanogr. 33, 2504–2526. doi:10.1175/1520-0485(2003)033<2504:NASWTH>2.0.CO;2

Chen, Q., Wang, L., Tawes, R., 2008. Hydrodynamic response of northeastern Gulf of Mexico to hurricanes. Estuaries and Coasts 31, 1098–1116.

Chen, Q., Zhao, H., Hu, K., Douglass, S.L., 2005. Prediction of wind waves in a shallow estuary. J. Waterw. port, coastal, Ocean Eng. 131, 137–148.

Coleman, J.M., Roberts, H.H., Stone, G.W., Coleman, J.M., Roberts, H.H., 1998. Mississippi River delta: an overview. Source J. Coast. Res. J. Coast. Res. Journ Res. 14, 698–716.

Corbett, D.R., McKee, B., Duncan, D., 2004. An evaluation of mobile mud dynamics in the Mississippi River deltaic region. Mar. Geol. 209, 91–112. doi:10.1016/j.margeo.2004.05.028

Dail, M.B., Reide Corbett, D., Walsh, J.P., 2007. Assessing the importance of tropical cyclones on continental margin sedimentation in the Mississippi delta region. Cont. Shelf Res. 27, 1857–1874. doi:10.1016/j.csr.2007.03.004

Egbert, G.D., Erofeeva, S.Y., 2002. Efficient inverse modeling of barotropic ocean tides. J. Atmos. Ocean. Technol. 19, 183–204. doi:10.1175/1520-0426(2002)019<0183:EIMOBO>2.0.CO;2

Elgar, S., Raubenheimer, B., 2008. Wave dissipation by muddy seafloors. Geophys. Res. Lett. 35, 1–5. doi:10.1029/2008GL033245

Ellwood, B.B., Balsam, W.L., Roberts, H.H., 2006. Gulf of Mexico sediment sources and sediment transport trends from magnetic susceptibility measurements of surface samples. Mar. Geol. 230, 237–248. doi:10.1016/j.margeo.2006.05.008

Flather, R.A., 1976. A tidal model of the northwest European continental shelf. Mem. Soc. Roy. Sci. Liege 10, 141–164.

Forbes, C., Luettich, R. A., Mattocks, C. A., Westerink, J.J., 2010. A retrospective evaluation of the storm surge produced by hurricane Gustav (2008): forecast and hindcast results. Weather Forecast. 25, 1577–1602. doi:10.1175/2010WAF2222416.1

Goñi, M.A., Alleau, Y., Corbett, R., Walsh, J.P., Mallinson, D., Allison, M.A., Gordon, E.S., Petsch, S., Dellapenna, T.M., 2007. The effects of Hurricanes Katrina and Rita on the seabed on the Louisiana shelf. Sediment. Rec. 5, 4–9.

Goñi, M.A., Gordon, E.S., Monacci, N.M., Clinton, R., Gisewhite, R., Allison, M.A., Kineke, G., 2006. The effect of Hurricane Lili on the distribution of organic matter along the inner Louisiana shelf (Gulf of Mexico, USA). Cont. Shelf Res. 26, 2260–2280. doi:10.1016/j.csr.2006.07.017

Haidvogel, D.B., Arango, H., Budgell, W.P., Cornuelle, B.D., Curchitser, E., Di Lorenzo, E., Fennel, K., Geyer, W.R., Hermann, A.J., Lanerolle, L., Levin, J., McWilliams, J.C., Miller, A.J., Moore, A.M., Powell, T.M., Shchepetkin, A.F., Sherwood, C.R., Signell, R.P., Warner, J.C., Wilkin, J., 2008. Ocean forecasting in terrain-following coordinates: Formulation and skill assessment of the Regional Ocean Modeling System. J. Comput. Phys. 227, 3595–3624. doi:10.1016/j.jcp.2007.06.016

Hoefel, F., Elgar, S., 2003. Wave-induced sediment transport and sandbar migration. Science 299, 1885–1887.

Hong, S.Y., Lim, J.O.J., 2006. The WRF single-moment 6-class microphysics scheme (WSM6). J. Korean Meteor. Soc 42, 129–151.

Hsu, T.J., Elgar, S., Guza, R.T., 2006. Wave-induced sediment transport and onshore sandbar migration. Coast. Eng. 53, 817–824. doi:10.1016/j.coastaleng.2006.04.003

Hu, K., Chen, Q., 2011. Directional spectra of hurricane-generated waves in the Gulf of Mexico. Geophys. Res. Lett. 38.

Iacono, M.J., Delamere, J.S., Mlawer, E.J., Shephard, M.W., Clough, S.A., Collins, W.D., 2008. Radiative forcing by long-lived greenhouse gases: Calculations with the AER radiative transfer models. J. Geophys. Res. Atmos. 113, 2–9. doi:10.1029/2008JD009944

Jacob, R., Larson, J., Everest, O., 2005. M x N communication and parallel interpolation in Community Climate System Model Version 3 using the Model Coupling Toolkit. Int. J. High Perform. Comput. Appl. 19, 293–307. doi:10.1177/1094342005056116

Janjic, Z.I., 2002. Nonsingular implementation of the Mellor-Yamada Level 2.5 scheme in the NCEP Meso model. NCEP Off. Note 437, 61.

Jones, P., 1997. A user’s guide for SCRIP: A spherical coordinate remapping and interpolation package. Los Alamos Natl. Lab.

Keen, T.R., Bentley, S.J., Chad Vaughan, W., Blain, C.A., 2004. The generation and preservation of multiple hurricane beds in the northern Gulf of Mexico. Mar. Geol. 210, 79–105. doi:10.1016/j.margeo.2004.05.022

Keen, T.R., Glenn, S.M., 2002. Predicting bed scour on the continental shelf during Hurricane Andrew. J. Waterw. Port Coast. Ocean Eng. 128, 249–257. doi:10.1061/(ASCE)0733-950X(2002)128:6(249)

Keim, B.D., Muller, R.A., Stone, G.W., 2007. Spatiotemporal patterns and return periods of tropical storm and hurricane strikes from Texas to Maine. J. Clim. 20, 3498–3509. doi:10.1175/JCLI4187.1

Kumar, N., Voulgaris, G., Warner, J.C., Olabarrieta, M., 2012. Implementation of the vortex force formalism in the coupled ocean-atmosphere-wave-sediment transport (COAWST) modeling system for inner shelf and surf zone applications. Ocean Model. 47, 65–95. doi:10.1016/j.ocemod.2012.01.003

Lapetina, A., Sheng, Y.P., 2015. Simulating complex storm surge dynamics: Three-dimensionality, vegetation effect, and onshore sediment transport. J. Geophys. Res. Ocean. 120, 7363–7380.

Lesser, G.R., Roelvink, J.A., van Kester, J.A.T.M., Stelling, G.S., 2004. Development and validation of a three-dimensional morphological model. Coast. Eng. 51, 883–915. doi:10.1016/j.coastaleng.2004.07.014

Liu, K., Chen, Q., Hu, K., Xu, K., 2015. Numerical simulations of sediment deposition and erosion on Louisiana coast during hurricane Gustav, in: The Proceedings of the Coastal Sediments 2015. World Scientific, pp. 1–14.

Liu, K., Fearn, M.L., 1993. Lake-sediment record of late Holocene hurricane. Geology 21, 793–796. doi:10.1130/0091-7613(1993)021<0793

Liu, K.B., Li, C., Bianchette, T. A, McCloskey, T. A, Yao, Q., Weeks, E., 2011. Storm deposition in a coastal backbarrier lake in Louisiana caused by hurricanes Gustav and Ike. J. Coast. Res. 1866–1870.

Madsen, O.S., 1994. Spectral wave-current bottom boundary layer flows. Coast. Eng. Proc. 1, 384–398. doi:10.9753/icce.v24.

Madsen, O.S., Poon, Y.K., Graber, H.C., 1988. Spectral wave attenuation by bottom friction: Theory, paper presented at 21st International Conference on Coastal Engineering. Am. Soc. Civ. Eng., Torremolinos, Spain 492–504.

McAdoo, B.G., Pratson, L.F., Orange, D.L., 2000. Submarine landslide geomorphology, US continental slope. Mar. Geol. 169, 103–136. doi:10.1016/S0025-3227(00)00050-5

Meade, R.H., Moody, J.A., 2010. Causes for the decline of suspended-sediment discharge in the Mississippi River system, 1940–2007. Hydrol. Process. 24, 35–49.

Mickey, R., Xu, K., Libes, S., Hill, J., 2015. Sediment texture, erodibility, and composition in the Northern Gulf of Mexico and their potential impacts on hypoxia formation. Ocean Dyn. 65, 269.

Miles, T., Seroka, G., Kohut, J., Schofield, O., Glenn, S., 2015. Glider observations and modeling of sediment transport in Hurricane Sandy. J. Geophys. Res. C Ocean. 120, 1771–1791. doi:10.1002/2014JC010474

Nodine, M., Gilbert, R., Kiureghian, S., Cheon, J., Wrzyszczynski, M., Coyne, M., Ward, E., 2007. Impact of hurricane-induced mudslides on pipelines (OTC-18983-MS). Offshore Technol. Conf. 70, 1–13. doi:10.4043/18983-MS

Ogston, A.S., Sternberg, R.W., 1999. Sediment-transport events on the northern California continental shelf. Mar. Geol. 154, 69–82. doi:10.1016/S0025-3227(98)00104-2

Olabarrieta, M., Warner, J.C., Armstrong, B., Zambon, J.B., He, R., 2012. Ocean-atmosphere dynamics during Hurricane Ida and Nor'Ida: An application of the coupled ocean-atmosphere-wave-sediment transport (COAWST) modeling system. Ocean Modelling. 43–44, 112–137. doi:10.1016/j.ocemod.2011.12.008

Olabarrieta, M., Warner, J.C., Kumar, N., 2011. Wave-current interaction in Willapa Bay. J. Geophys. Res. Ocean. 116, 1–27. doi:10.1029/2011JC007387

Osterman, L.E., Poore, R.Z., Swarzenski, P.W., Senn, D.B., DiMarco, S.F., 2009. The 20th-century development and expansion of Louisiana shelf hypoxia, Gulf of Mexico. Geo-Marine Lett. 29, 405–414. doi:10.1007/s00367-009-0158-2

Palaseanu-Lovejoy, M., Kranenburg, C., Barras, J.A., Brock, J.C., 2013. Land loss due to recent hurricanes in coastal Louisiana, U.S.A. J. Coast. Res. 63, 97–109. doi:10.2112/SI63-009.1

Palinkas, C.M., Halka, J.P., Li, M., Sanford, L.P., Cheng, P., 2013. Sediment deposition from tropical storms in the upper Chesapeake Bay: Field observations and model simulations. Cont. Shelf Res. 1–11. doi:10.1016/j.csr.2013.09.012

Parchure, T.M., Mehta, A.J., 1985. Erosion of soft cohesive sediment deposits. J. Hydraul. Eng. 111, 1308–1326.

Price, J.F., 1981. Upper ocean response to a hurricane. J. Phys. Oceanogr. doi:10.1175/1520-0485(1981)011<0153:UORTAH>2.0.CO;2

Rinehimer, J.P., Harris, C.K., Sherwood, C.R., Sanford, L.P., 2008. Estimating cohesive sediment erosion and consolidation in a muddy, tidally-dominated environment: Model behavior and sensitivity, in: Estuarine and Coastal Modeling (2007). pp. 819–838.

Rong, Z., Hetland, R.D., Zhang, W., Zhang, X., 2014. Current-wave interaction in the Mississippi-Atchafalaya river plume on the Texas-Louisiana shelf. Ocean Model. 84, 67–83. doi:10.1016/j.ocemod.2014.09.008

Shay, L.K., Black, P.G., Mariano, A.J., Hawkins, J.D., Elsberry, R.L., 1992. Upper ocean response to Hurricane Gilbert. J. Geophys. Res. 97, 20227. doi:10.1029/92JC01586

Shchepetkin, A.F., McWilliams, J.C., 2005. The regional oceanic modeling system (ROMS): A split-explicit, free-surface, topography-following-coordinate oceanic model. Ocean Model. 9, 347–404. doi:10.1016/j.ocemod.2004.08.002

Sheng, Y.P., Alymov, V., Paramygin, V.A., 2010. Simulation of storm surge, wave, currents, and inundation in the outer banks and Chesapeake Bay during Hurricane Isabel in 2003: The importance of waves. J. Geophys. Res. Ocean. 115, 1–27. doi:10.1029/2009JC005402

Sheremet, A., Mehta, A.J., Liu, B., Stone, G.W., 2005. Wave-sediment interaction on a muddy inner shelf during Hurricane Claudette. Estuar. Coast. Shelf Sci. 63, 225–233. doi:10.1016/j.ecss.2004.11.017

Skamarock, W.C., Klemp, J.B., Dudhi, J., Gill, D.O., Barker, D.M., Duda, M.G., Huang, X.-Y., Wang, W., Powers, J.G., 2005. A description of the Advanced Research WRF Version 3. Tech. Rep. 113. doi:10.5065/D6DZ069T

Stone, G.W., Xu, J.P., Zhang, X., 1995. Estimation of the wave field during hurricane Andrew and morphological change along the Louisiana coast. J. Coast. Res. 21, 234–253.

Taylor, P.K., Yelland, M.J., 2001. The dependence of sea surface roughness on the height and steepness of the waves. J. Phys. Oceanogr. 31, 572–590. doi:10.1175/1520-0485(2001)031<0572:TDOSSR>2.0.CO;2

Teague, W.J., Jarosz, E., Wang, D.W., Mitchell, D.A., 2007. Observed oceanic response over the upper continental slope and outer shelf during hurricane Ivan. J. Phys. Oceanogr. 37, 2181–2206. doi:10.1175/JPO3115.1

Tewari, M., Chen, F., Wang, W., Dudhia, J., LeMone, M.A., Mitchell, K., Ek, M., Gayno, G., Wegiel, J., Cuenca, R.H., 2004. Implementation and verification of the unified NOAH land surface model in the WRF model, in: 20th Conference on Weather Analysis and forecasting/16th Conference on Numerical Weather Prediction.

Thornton, E.B., Guza, R.T., 1983. Transformation of wave height distribution. J. Geophys. Res. 88, 5925. doi:10.1029/JC088iC10p05925

Turner, R.E., Baustian, J.J., Swenson, E.M., Spicer, J.S., 2006. Wetland sedimentation from hurricanes Katrina and Rita. Science (80-.). 314, 449–452. doi:10.1126/science.1129116

Turner, R.E., Swenson, E.M., Milan, C.S., Lee, J.M., 2007. Hurricane signals in salt marsh sediments: Inorganic sources and soil volume. Limnol. Oceanogr. 52, 1231–1238. doi:10.4319/lo.2007.52.3.1231

Uchiyama, Y., McWilliams, J.C., Shchepetkin, A.F., 2010. Wave-current interaction in an oceanic circulation model with a vortex-force formalism: Application to the surf zone. Ocean Model. 34, 16–35. doi:10.1016/j.ocemod.2010.04.002

Uhlhorn, E.W., Klotz, B.W., Vukicevic, T., Reasor, P.D., Rogers, R.F., 2014. Observed hurricane wind speed asymmetries and relationships to motion and environmental shear. Mon. Weather Rev. 142, 1290–1311. doi:10.1175/MWR-D-13-00249.1

Walker, N.D., 2001. Tropical storm and hurricane wind effects on water level, salinity, and sediment transport in the river-influenced Atchafalaya-Vermilion Bay system, Louisiana, USA. Estuaries 24, 498–508.

Walker, N.D., Hammack, A.B., 2000. Impacts of winter storms on circulation and sediment transport: Atchafalaya-Vermilion Bay region, Louisiana, USA. J. Coast. Res. 996–1010.

Walker, N.D., Leben, R.R., Balasubramanian, S., 2005. Hurricane-forced upwelling and chlorophyll a enhancement within cold-core cyclones in the Gulf of Mexico. Geophys. Res. Lett. 32, 1–5. doi:10.1029/2005GL023716

Walsh, J.P., Corbett, D.R., Mallinson, D., Goni, M., Dail, M., Loewy, K., Marciniak, K., Ryan, K., Smith, C., Stevens, A., Sumners, B., Tesi, T., 2006. Mississippi delta mudflow activity and 2005 gulf hurricanes. Eos (Washington. DC). 87, 30–32. doi:10.1029/2006EO440002

Warner, J.C., Armstrong, B., He, R., Zambon, J.B., 2010. Development of a Coupled Ocean-Atmosphere-Wave-Sediment Transport (COAWST) modeling system. Ocean Model. 35, 230–244. doi:10.1016/j.ocemod.2010.07.010

Warner, J.C., Sherwood, C.R., Signell, R.P., Harris, C.K., Arango, H.G., 2008. Development of a three-dimensional, regional, coupled wave, current, and sediment-transport model. Comput. Geosci. 34, 1284–1306. doi:10.1016/j.cageo.2008.02.012

Williams, H.F.L., Flanagan, W.M., 2009. Contribution of hurricane Rita storm surge deposition to long-term sedimentation in Louisiana coastal woodlands and marshes. J. Coast. Res. 2009, 1671–1675.

Willmott, C., 1982. Some comments on the evaluation of model performance. Bull. Am. Meteorol. Soc. doi:10.1175/1520-0477(1982)063<1309:SCOTEO>2.0.CO;2

Xie, L., Liu, H., Liu, B., Bao, S., 2011. A numerical study of the effect of hurricane wind asymmetry on storm surge and inundation. Ocean Model. 36, 71–79. doi:10.1016/j.ocemod.2010.10.001

Xu, K., Harris, C.K., Hetland, R.D., Kaihatu, J.M., 2011. Dispersal of Mississippi and Atchafalaya sediment on the Texas-Louisiana shelf: Model estimates for the year 1993. Cont. Shelf Res. 31, 1558–1575. doi:10.1016/j.csr.2011.05.008

Xu, K., Mickey, R.C., Chen, Q., Harris, C.K., Hetland, R.D., Hu, K., Wang, J., 2016. Shelf sediment transport during hurricanes Katrina and Rita. Comput. Geosci. 90, 24–39. doi:10.1016/j.cageo.2015.10.009

Yoon, B., Raymond, P.A., 2012. Dissolved organic matter export from a forested watershed during Hurricane Irene. Geophys. Res. Lett. 39, 1–6. doi:10.1029/2012GL052785

Zambon, J.B., He, R., Warner, J.C., 2014. Investigation of hurricane Ivan using the coupled ocean-atmosphere-wave-sediment transport (COAWST) model. Ocean Dyn. 64, 1535–1554. doi:10.1007/s10236-014-0777-7

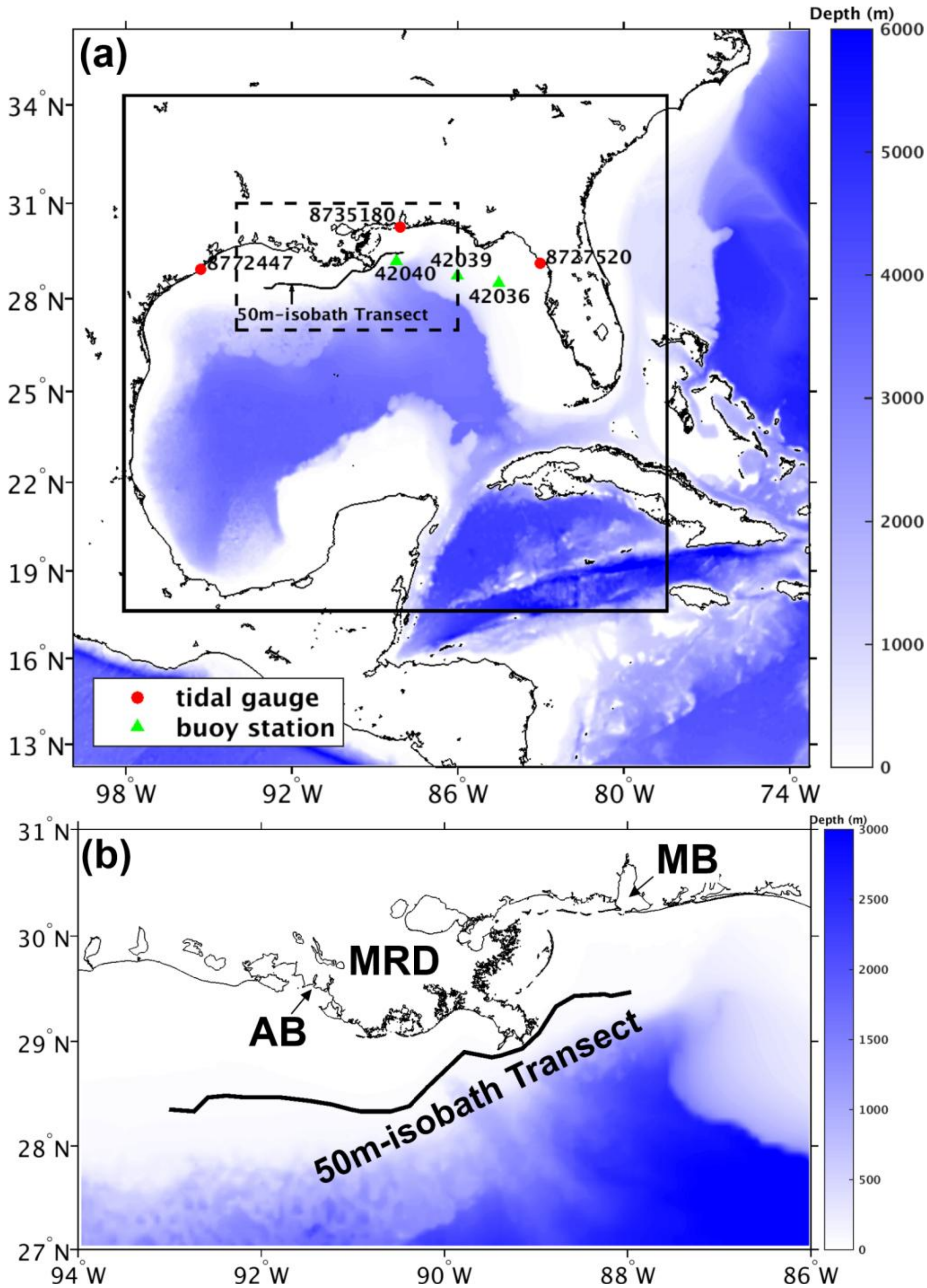

Fig. 1. Grid domain used in the WRF overlaid with the water depth (color shading), locations of tide gauges (red circle), buoy stations (green triangle), and 50 m isobath transect (black line). The black solid box represents the domain used in ROMS and SWAN, and the black dashed box represents the northern Gulf of Mexico (nGoM) region focused on in this study. More details regarding nGoM and the transect locations are shown in the lower panel. AB: Atchafalaya Bay; MRD: Mississippi River Delta; MB: Mobile Bay.

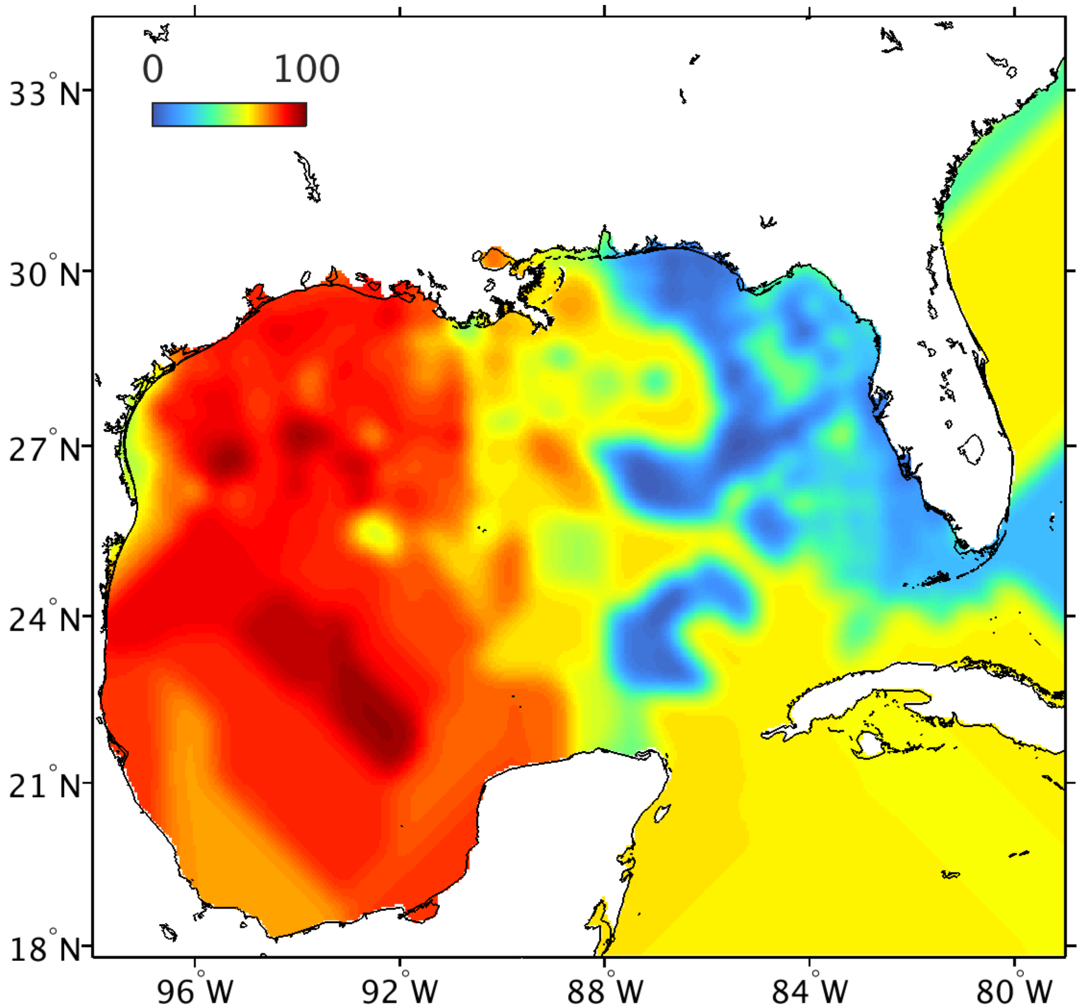

Fig. 2. Mud fraction distributions (%) on the seafloor derived from usSEABED datasets (Buczkowski, 2006).

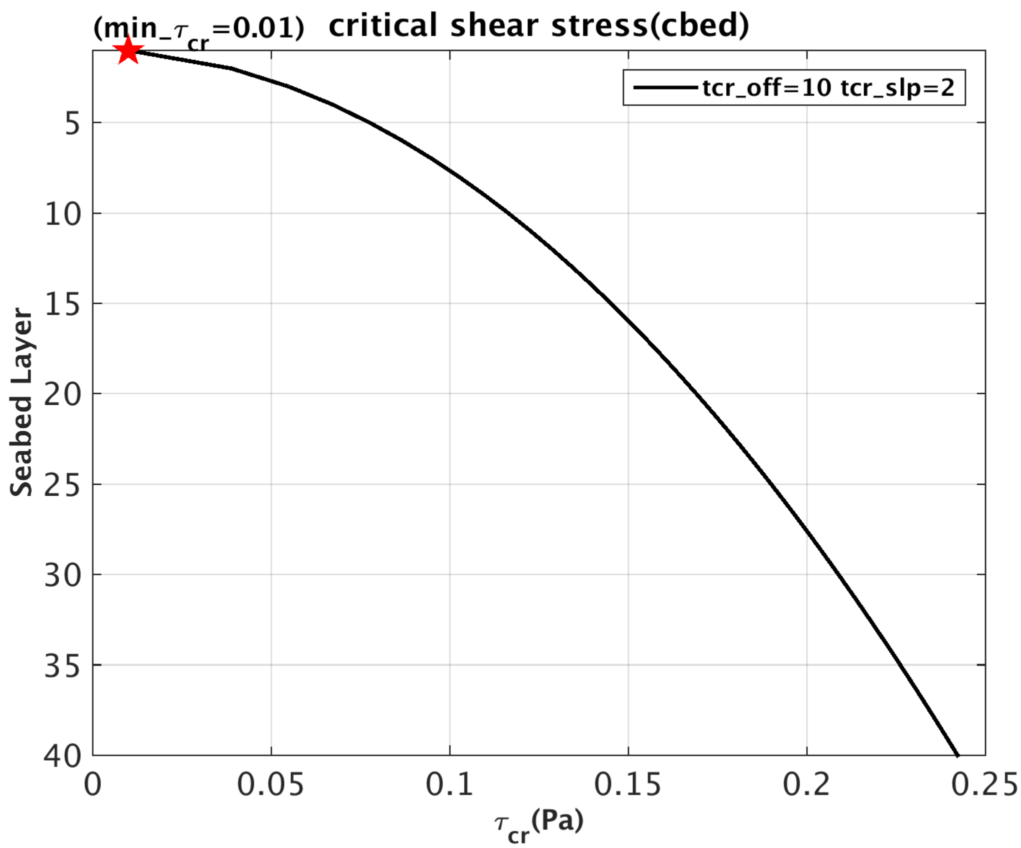

Fig. 3. Equilibrium critical shear stress profile designed for the initial sediment conditions on August 30, 2008. The red star represents the minimum critical shear stress (min_τ_{cr} = 0.01 Pa) in the top layer.

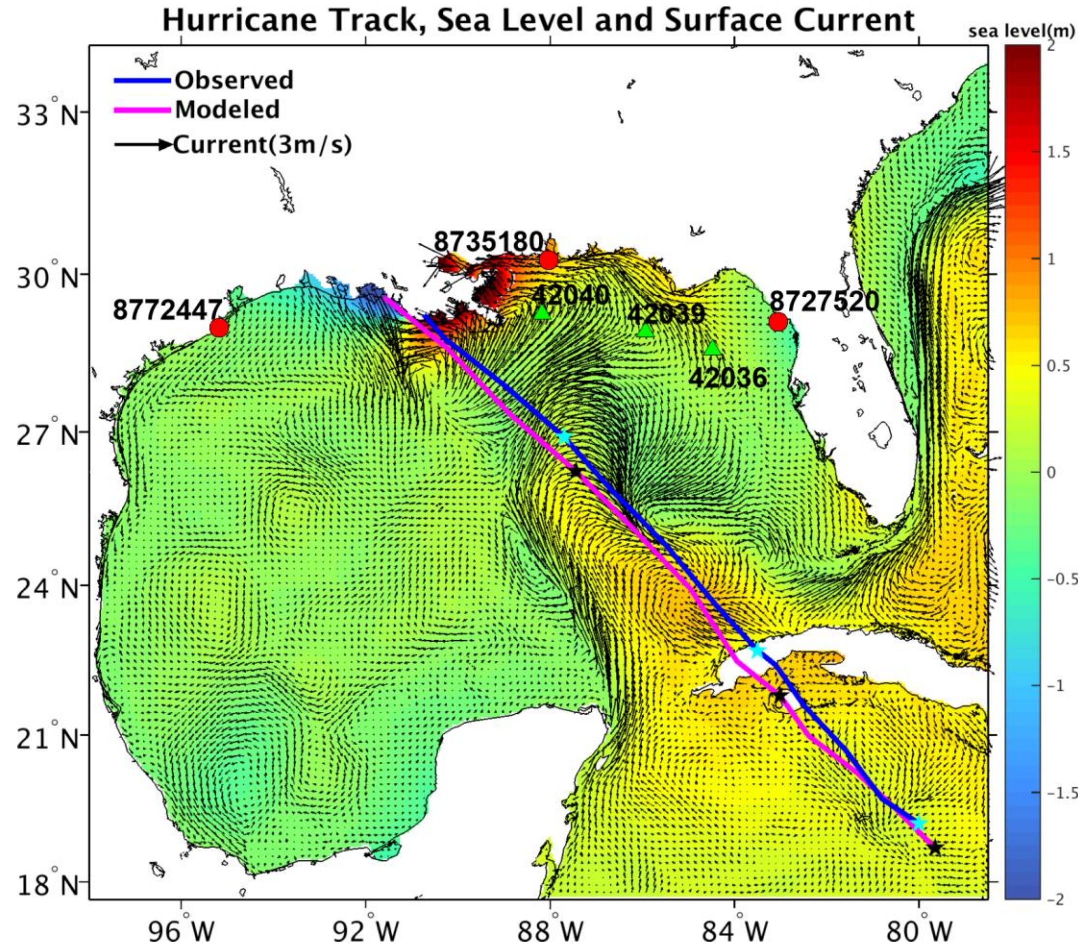

Fig. 4. Surface current fields (arrow) and sea level (color) at 1600 UTC September 1, and a comparison of the simulated and observed tracks of Hurricane Gustav (2008). The black (modeled) and cyan (observed) stars from southeast to northwest represent the locations of the tropical cyclone eye at 0000 UTC on August 30, 31, and September 1. Buoy stations and tide gauges are also shown.

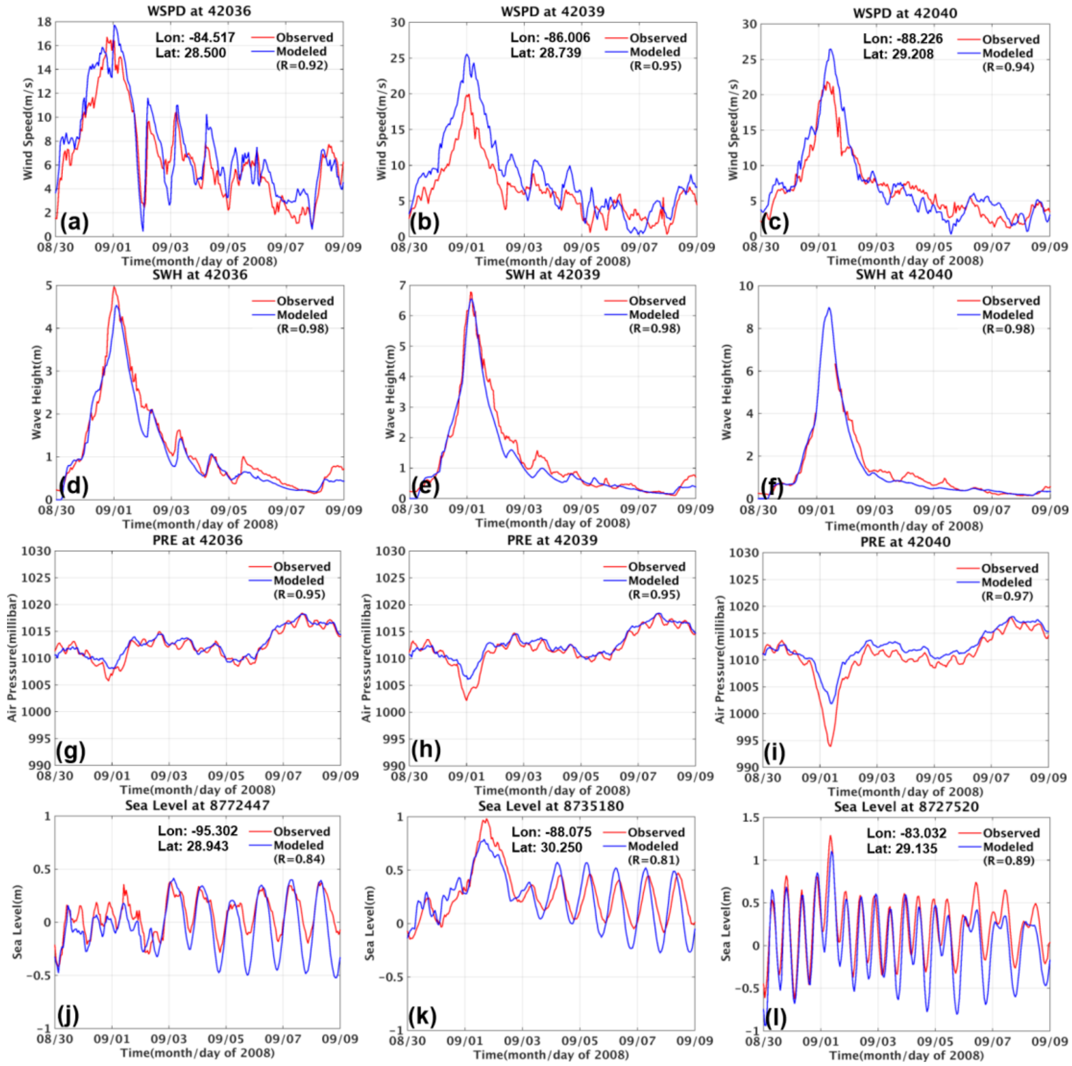

Fig. 5. Comparisons of the observed and simulated wind speed, significant wave height, air pressure, and sea level anomaly during the passage of hurricane Gustav (2008).

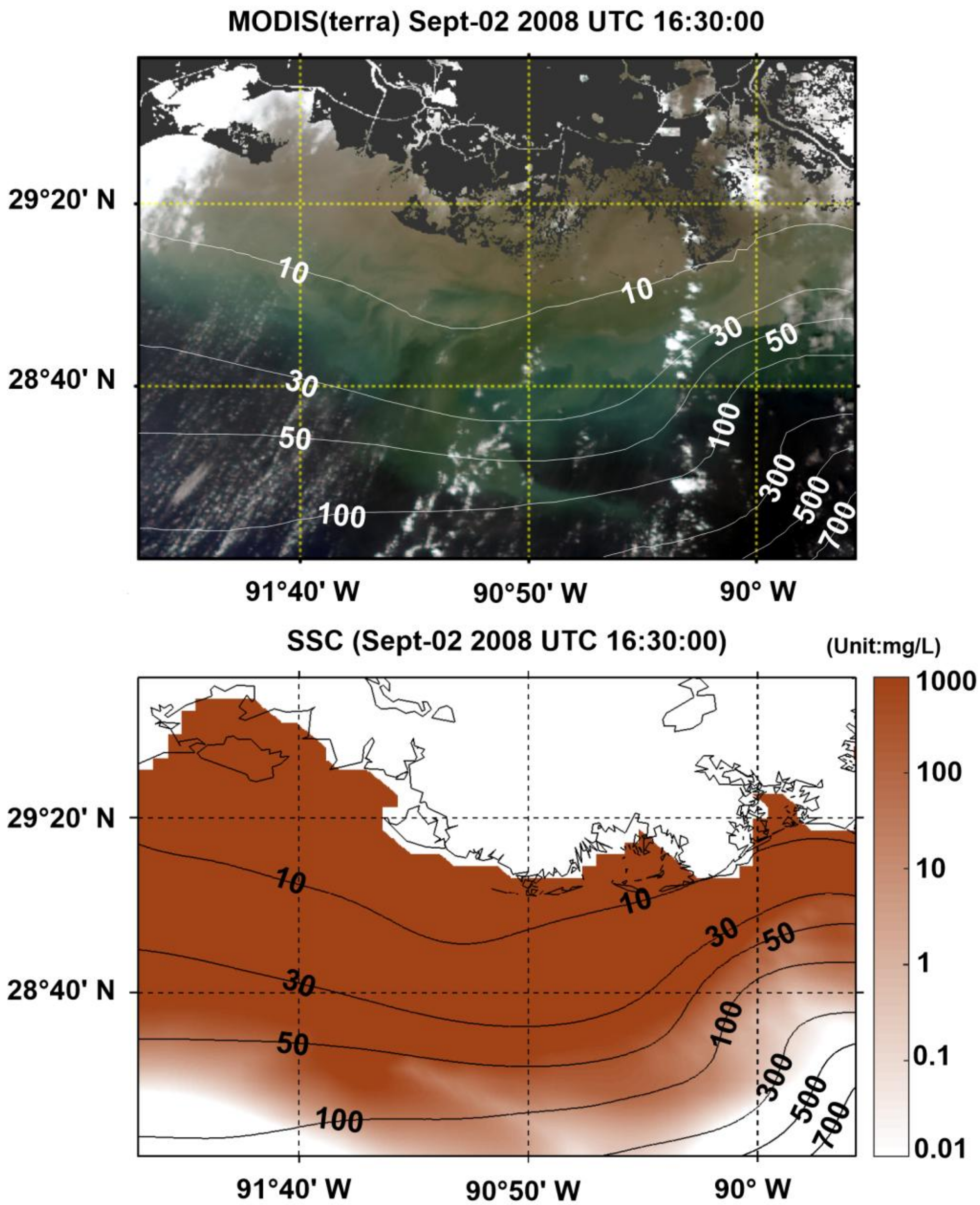

Fig. 6. Comparison of the MODIS Terra true-color image and simulated SSC at 16:30:00 UTC on September 2, 2008.

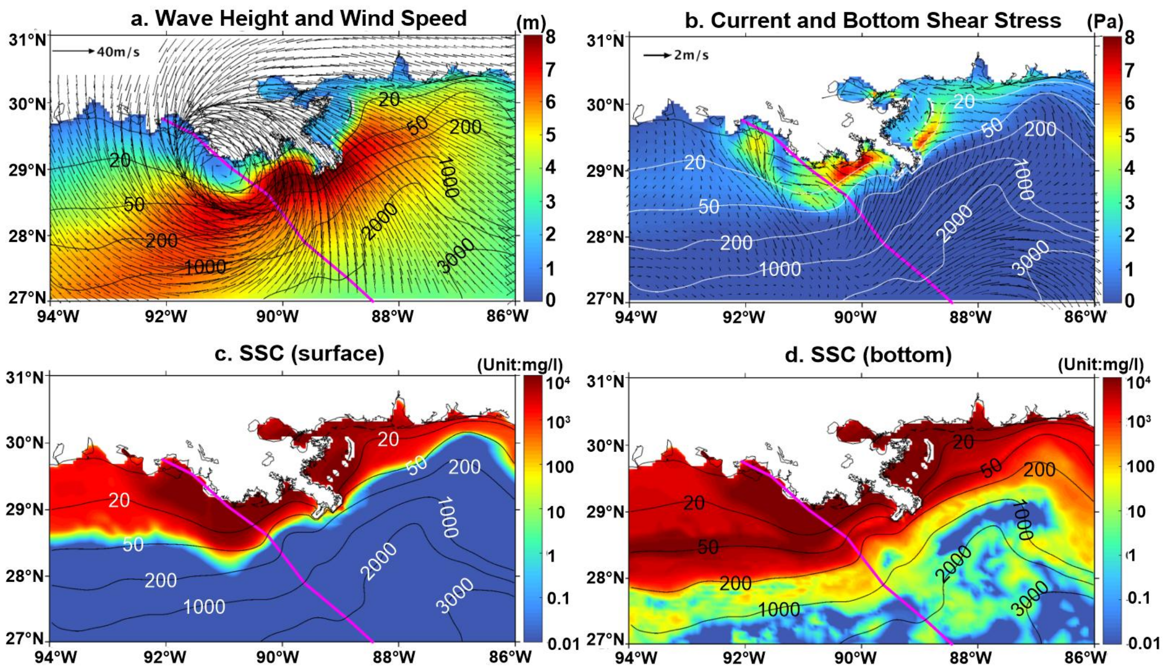

Fig. 7. Maps showing the (a) wind (arrow) and significant wave height (color) fields, (b) surface currents (arrow) and bottom shear stress induced by the currents and waves (color), (c) surface SSC, and (d) bottom SSC during the landing of Gustav. The simulated track line is also shown (magenta).

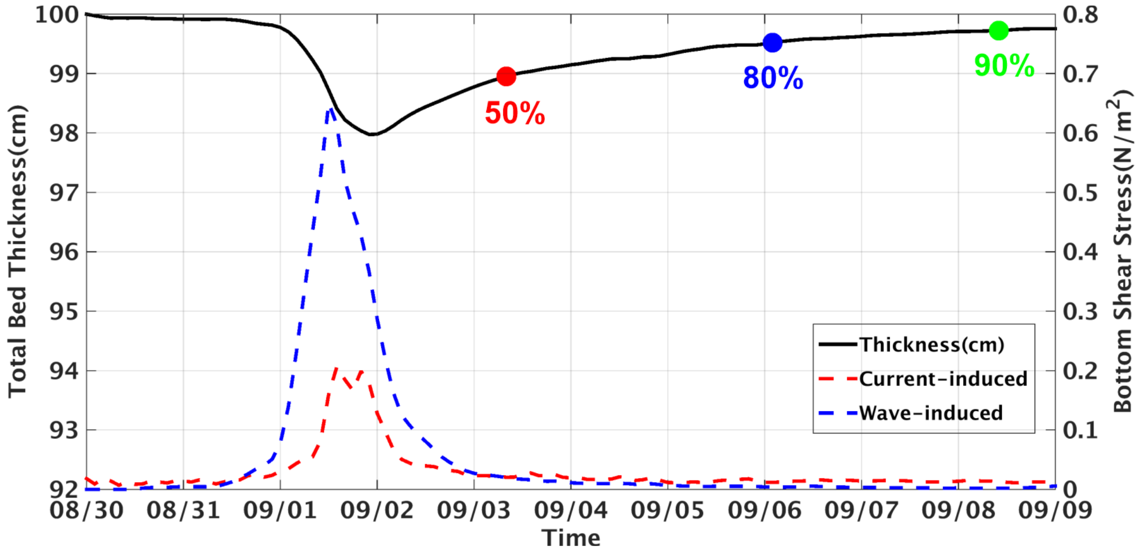

Fig. 8. Time series of spatial averaged (nGoM) current-induced bottom shear stress (red dashed line), wave-induced bottom shear stress (blue dashed line), and bed thickness (black solid line). Red, blue, and green dots represent 50%, 80%, and 90% of the hurricane-induced suspended sediment settling back on the seafloor, respectively.

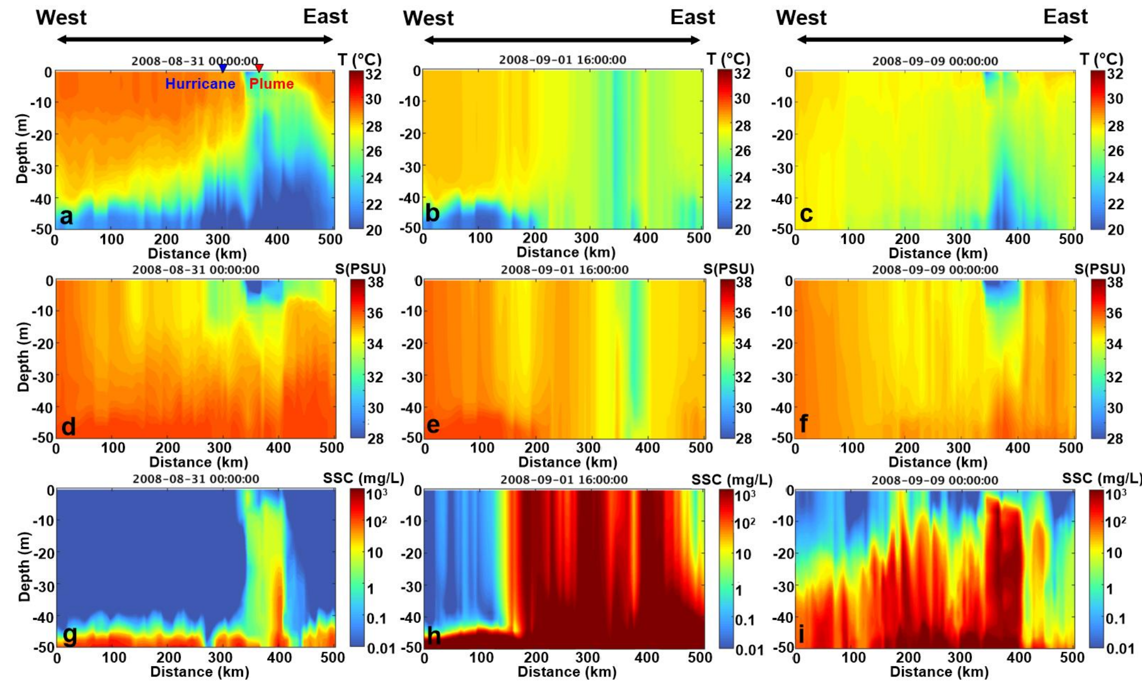

Fig. 9. Vertical distributions of temperature (a, b, and c), salinity (d, e, and f), and suspended sediment concentration (SSC) (g, h, and i) at the 50-m isobath transect (the location is shown in Fig. 1) during the passage of hurricane Gustav (2008). The first, second, and third columns represent the conditions at 0000 UTC on August 31 (pre-hurricane), 1600 UTC on September 1 (during-hurricane), and 0000 UTC on September 9 (post-hurricane), respectively. The red and blue triangles in the upper left panel illustrate the locations of the river plume and the intersection of the hurricane trackline and transect.

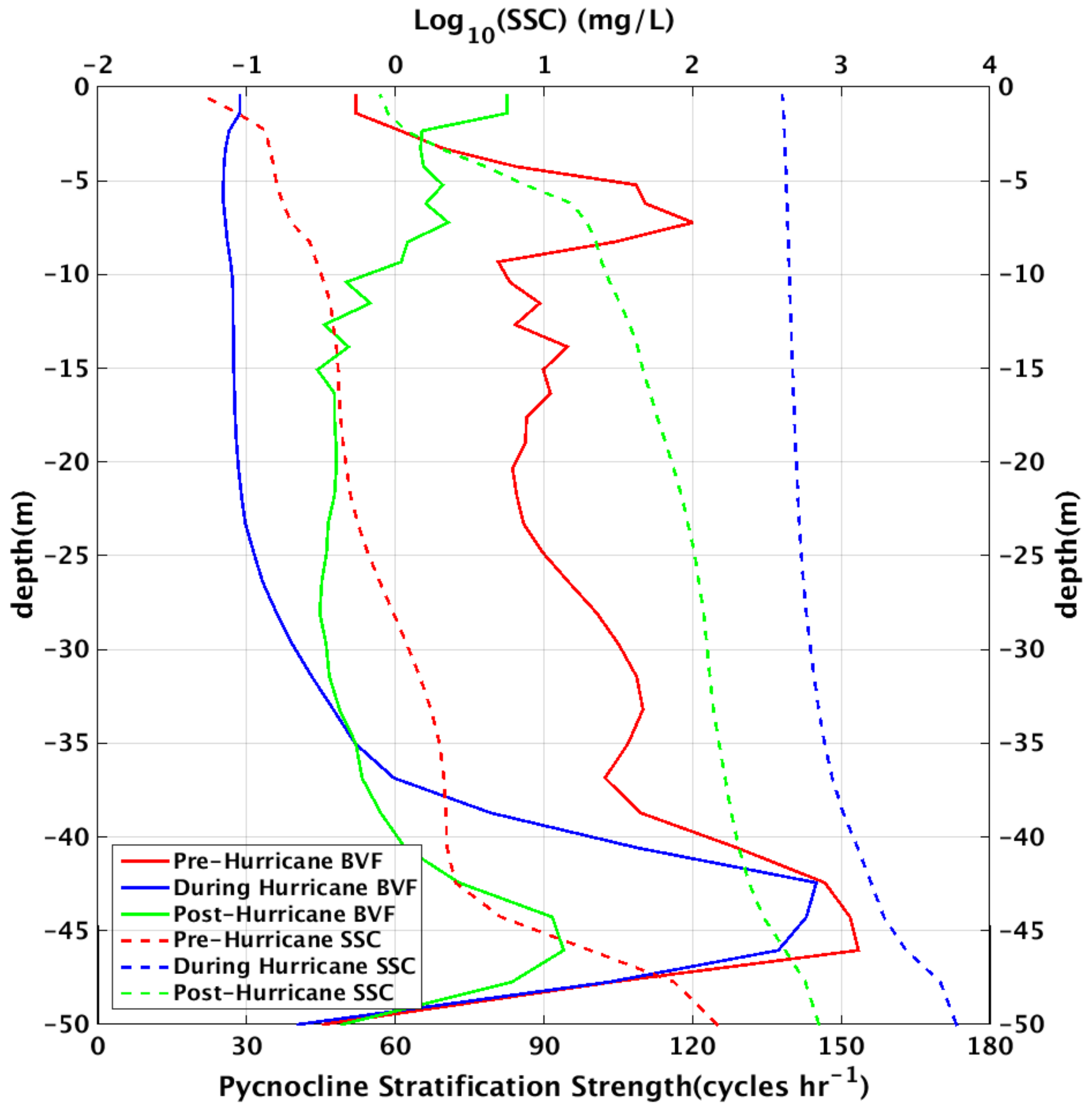

Fig. 10. Vertical distributions of the modeled mean Brunt Väisälä Frequency (BVF) and SSC along the 50-m isobath transect (the location is shown in Fig. 1).

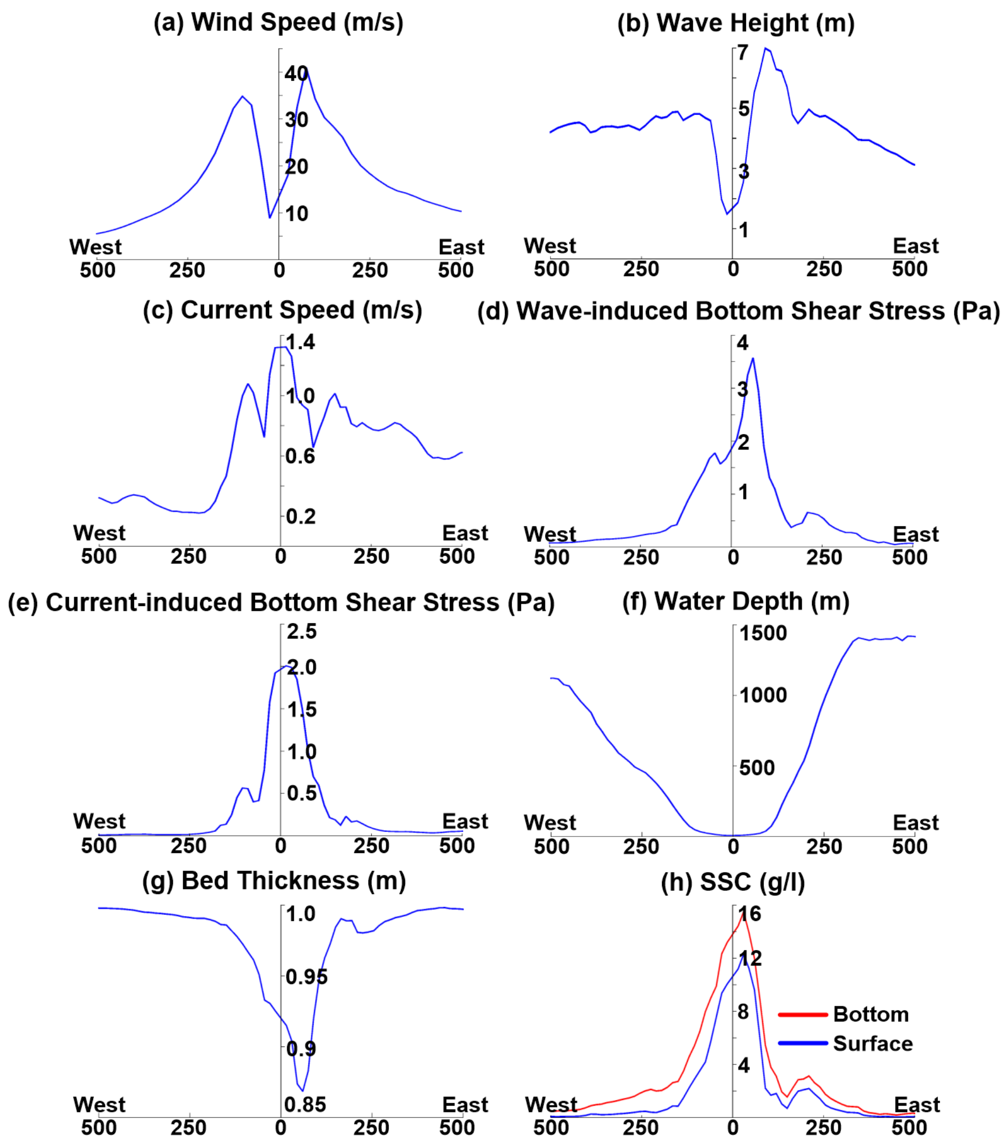

Fig. 11. Variations in the wind speed (a), significant wave height (b), surface current speed (c), wave-induced bottom shear stress (d), current-induced bottom shear stress (e), water depth (f), bed thickness (g), and SSC (h) at 16:00:00 UTC, September 1, with distance from the hurricane center when it made landfall.

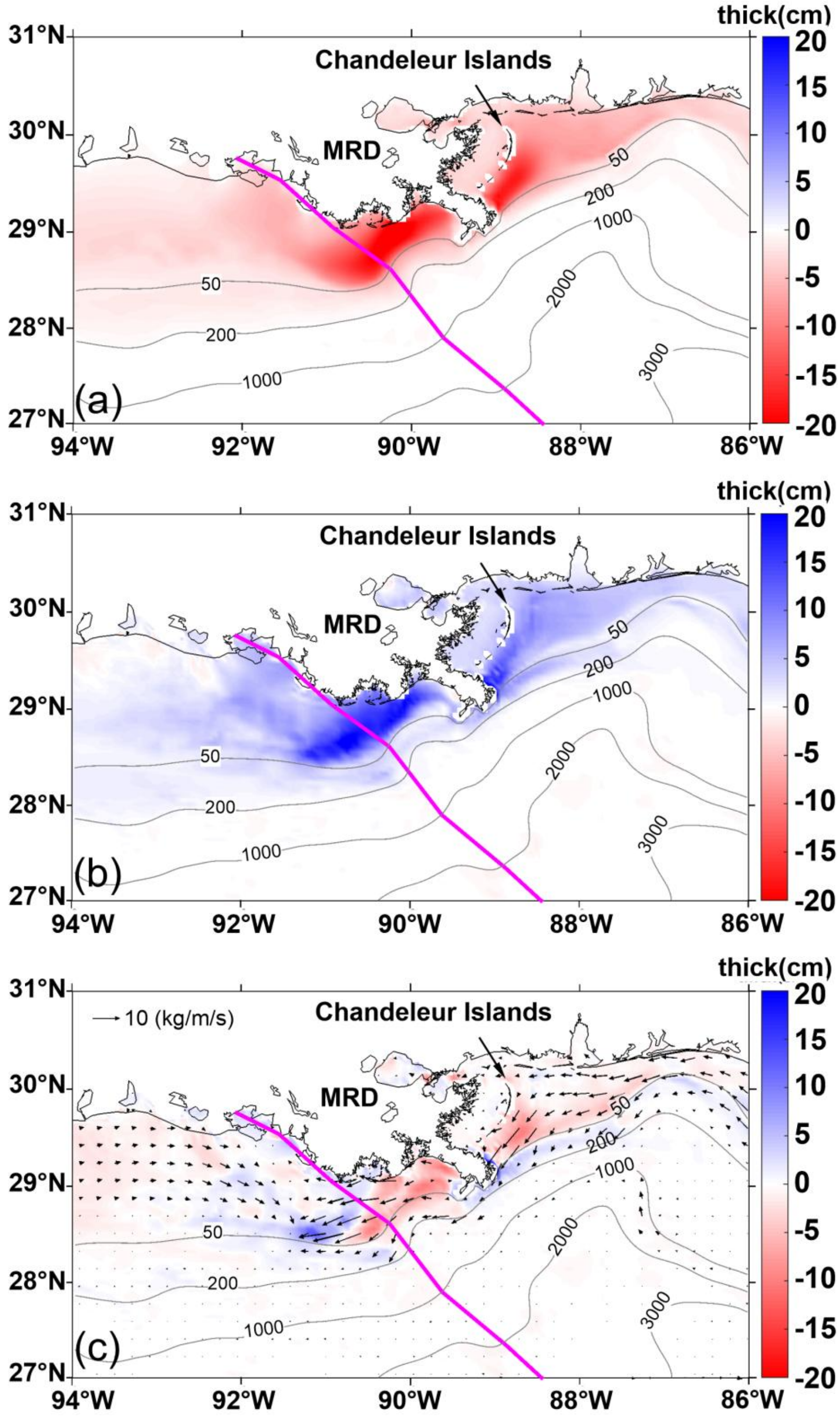

Fig. 12. Distributions of maximum erosion (a), post-hurricane deposition (b), and net erosion/deposition (c) during the simulation period. Arrows in (c) indicate the depth-integrated and time-averaged suspended sediment flux. MRD: Mississippi River Delta.

Table 1 Characteristic sediment parameters

	Grain diameter (mm)	Settling velocity (mm/s)	Grain density (kg/m^3)	Erosion rate (10^{-4} $kg/m^2/s$)
Mud_01(fluvial&seabed)	0.004	0.1	2650	5
Mud_02(fluvial&seabed)	0.03	0.1	2650	5
Sand_01(fluvial&seabed)	0.0625	1	2650	5
Sand_02(seabed)	0.14	1	2650	5